Novel High-Brightness Extreme/Vacuum Ultraviolet Excimer Light Source for ARPES

by

Eric G. Miller

A thesis submitted to the

Honors Council of the University of Colorado-Boulder

in partial fulfillment of the requirements for the degree of

Bachelor of Arts

Department of Physics

April 2, 2014

This thesis entitled:
Novel High-Brightness Extreme/Vacuum Ultraviolet Excimer Light Source for ARPES
written by Eric G. Miller
has been approved for the Department of Physics

_____

Daniel S. Dessau

_____

Prof. James K. Thompson, Physics

_____

Prof. Paul M. Levitt, English

Date _____

The final copy of this thesis has been examined by the signatories, and we find that both the content and the form meet acceptable presentation standards of scholarly work in the above mentioned discipline.

Miller, Eric G. (B.A., Physics)

Novel High-Brightness Extreme/Vacuum Ultraviolet Excimer Light Source for ARPES

Thesis directed by Prof. Daniel S. Dessau

This thesis describes the construction and ongoing development of a novel CVD diamond-based excimer light source capable of generating a large range of high energy ultraviolet light, including Extreme and Vacuum UV light (EUV/VUV). First, I present some motivation, background, and some potential advantages to this novel system, then I provide a thorough description of the physical system, including all the considerations that must be made to build this system. Next, I provide a description of how to operate and characterize this system. Because this project is ongoing, the system has not yet been operated or characterized. Finally, I provide a description of future work following the characterization of this system. I also discuss what potential impact this novel light source could have on a few notable applications of the rapidly growing field of excimer technologies. This project is motivated by the desire for a high brightness UV source to be used by the Dessau group in Angle-Resolved Photoemission Spectroscopy.

Acknowledgements

I would like to thank Dan for giving me the opportunity to work on such an interesting project, as well as providing invaluable insight and resources regarding this project. I would like to thank Justin Griffith for imagining the use of diamond as a membrane between vacuum and excimer gas, as well as for lending me his insight in nearly every facet of this project and tolerating my incredibly persistent questions. I would like to thank Ryan Brow of the Colorado Nanofabrication Labs for his help and mentorship at CNL. I would also like to thank Dr. Bradford Pate for providing the diamond membranes for this project. Thank you Ben Bellman and Matt Kilpatrick for copy editing my thesis and allowing me to distract you from your respective honors theses. Thank you Steve, Justin, Xiaoqing, Haoxiang, Daniel, Scott, Sam, and the whole Dessau group for your help as well as creating an all-around awesome workplace environment. Finally, thank you Mom, Dad, Sam, Leah, Grandma, Poppie, and Chicago—the greatest city in the world—for helping me become the person I am today.

Contents

Chapter

Tables

Table

Figures

Figure

Chapter 1

Background

1.1 Experimental Basis

The experimental basis for this Novel High Brightness Extreme/Vacuum Ultraviolet Excimer Light Source (UV Light Source) is the well characterized field of Excimer Technology. The first example of excimer lasers was demonstrated in 1975, very shortly after the fluorescence spectra of rare gas halides were characterized, and the sector of Excimer technology has been rapidly expanding ever since [5]. This project's specific experimental basis comes from a German group who developed a compact and robust system for the generation of Extreme UV (EUV) and Vacuum UV (VUV) [15, 16]. The schematic design of this UV Light Source and the one described by the Mühlberger Group will be the same; the novelty of this UV Light Source lies in the choice of materials and preferred mode of operation.

Schematically, both systems consist of an electron beam incident on a thin film that transmits electrons between the necessary vacuum to generate high energy electrons and a chamber occupied by high-density noble gas (we will demonstrate proof of concept with Argon). When the electrons hit the gas, they form a short-lived **exc**ited d**imer** state (excimer) that then decays back down to a monatomic state by radiation. The energy of this transition is determined by the choice of gas, but all transitions—including those containing only one noble gas and those containing a mixture of gasses—radiate photons with wavelengths in the range 60-193 nm. The bandwidth of this transition is also dependent upon the choice of gas or gas mixture [15]. These energies lie within the range of EUV (121-10 nm) and VUV (200-10 nm) light [21], and as such the nature of this type of light

must be taken into consideration as the light generated is most easily used in vacuum.

The Mühlberger group designed their system for use in a mass spectrometry setting, whereas this UV Light Source will be used in an Angle-Resolved Photoemission Spectroscopy (ARPES) setting. Both the specifications and the form of this UV Light Source reflect this desired function. While the Mühlberger Group prioritized a compact system, this UV Light Source trades (to an extent) a smaller system size for higher photon intensity.

The Mühlberger system used a 300 nm thick 1 x 1 mm^2 silicon nitride (SiN) foil as the electron transmission membrane. However, this material fails in that the thermal stress applied is proportional to the average electron flux, and as such, operation of an electron beam in continuous-wave (CW) mode leads to the destruction of the SiN foil. Due to this proportionality, the Mühlberger group was able to achieve the highest intensities operating in a pulsed-wave (PW) mode [16]. This mode of operation was acceptable in the setting of mass spectroscopy, but for ARPES, we would like a light source in CW mode for reasons discussed in Section 1.4. To build a CW system, instead of using a SiN electron transmission membrane, this UV Light Source will use a 500 nm thick 1/2 mm diameter nano-crystalline Chemical Vapor Deposition diamond (ncCVD) as discussed in Section 2.3. Additionally a cooling system is added to the system (Section 2.5) to mitigate the thermal load deposited on the diamond by the electron beam.

1.2 Motivation

The field of Condensed Matter Physics studies the physics of matter in condensed phases—be they liquids, solids, or more exotic phases exhibited at low temperatures—using the fundamental laws of Quantum Mechanics, Statistical Mechanics, and Electromagnetism. The breadth of Condensed Matter Physics is massive, with topics ranging from Material Sciences to Quantum Gases to Neural Networks.

While this UV Light Source will be used to study many areas of interest in Condensed Matter, superconductivity is a particularly enlightening example as to how this technology will better the Dessau Group's current ARPES system. Superconductivity is of interest to Condensed

Matter physicists because superconductors exhibit miraculous properties such as exactly zero electrical resistance and the repulsion of all magnetic field lines. Condensed Matter Physicists seek to understand the mechanism by which superconductivity occurs so that superconductors might be used in future devices without the need for expensive cooling systems. While the phenomenon of superconductivity has been well characterized, there is no adequate theoretical description of superconductivity that describes all superconductors.

Currently, the theory that best describes superconductivity is the Bardeen-Cooper-Schrieffer (BCS) Theory, which states that a very small attractive potential between two fermions (I.E. electrons, Helium-3, baryons, etc.) caused by electron-phonon interactions in conventional superconductors allows two fermions to form a bound state known as a Cooper Pair [6]. This composite quasiparticle behaves like a boson, which means these fermion pairs are allowed to occupy the same ground state, a phenomenon previously disallowed by the Pauli Exclusion Principle. This pairing effectively allows electron pairs to resist kicks from oscillations in the conductor uniformly, causing the phenomenon of exactly zero resistance [4]. Cooper Pairing only occurs at sufficiently low temperatures, as very little thermal energy is required to break cooper bonds ($\sim 10^{-3}$ eV), which is why conventional (Type-I) superconductors must be cooled to a very low temperature ($\sim 10^{-2}$ K) to go superconducting.

However, BCS theory adequately describes only what are referred to as Type-I Superconductors. Type-I and Type-II superconductors are not only distinct in that Type-I superconductors must be much colder than Type-II in order to achieve superconductivity, but they are also distinct in their behavior as superconductors.

Type-II superconductors are drastically different than Type-I superconductors under a magnetic field. One of the unique and fascinating properties of superconductors is their tendency to repel all magnetic field lines, a property known as the Meissner Effect. In the case of Type-I superconductors, if a large enough magnetic field is applied while the material is held at a temperature below the temperature at which the material is superconducting (Critical Temperature, T_c), Type-I superconductors undergo a phase transition back into the normal state. Once the energy of the

magnetic field is greater than the cooper bonds, the cooper pairs are broken and electron behavior returns to its normal, fermion state. Type-II superconductors, however, do not behave this way. Instead, magnetic vortices open inside of the material that allow some magnetic field lines to pass through, even though the material is still in a superconducting state [1]. A better understanding of this mechanism and the mechanism that accounts for the High-T_c of some Type-II superconductors is just one of a multitude of motivations behind this UV Light Source, and as such, the value of this device is by no means limited to this study, or even condensed matter physics.

1.3 Angle-Resolved Photoemission Spectroscopy

Angle-Resolved Photoemission Spectroscopy (ARPES) is the mechanism by which we will study these Type-II superconductors—generally Bismuth strontium calcium copper oxide or BSCCO (pronounced "bisko"), one of the highest T_c superconductors known—as well as many other condensed matter topics of interest, and by understanding the ARPES mechanism, we in turn understand what will be gained with this UV light source.

The Dessau Group's ARPES setup (Figure 1.1) consists of a source of monochromatic light incident on a superconducting sample in Ultra-High Vacuum ($< 10^{-8}$ torr, where 1 atm = 760 torr). The light, which sweeps out the polar angle θ (hence, the "Angle-Resolved"), scatters electrons off of the sample and into a hemispherical detector that analyzes the energy and angle of the ejected electrons. The ARPES system is also capable of using an ultrafast pump-probe system with a 7 eV Titanium-Sapphire Laser as well as the 6 eV Ti:Sapphire Laser which operates in CW mode. ARPES is based on The Photoelectric Effect, first fully realized in Einstein's 1905 Nobel Prize winning paper. The Photoelectric Effect states that when photons are incident on atoms, atoms release electrons, called photoelectron. The maximum kinetic energy of those electrons is given by:

$$K_{max} = \hbar\omega - \phi = \hbar(\omega - \omega_0) \tag{1.1}$$

where K_{max} is the maximum photoelectron kinetic energy, ω is the angular frequency of the incident photon, and ϕ is the work function of the material, which may also be written in terms of a threshold

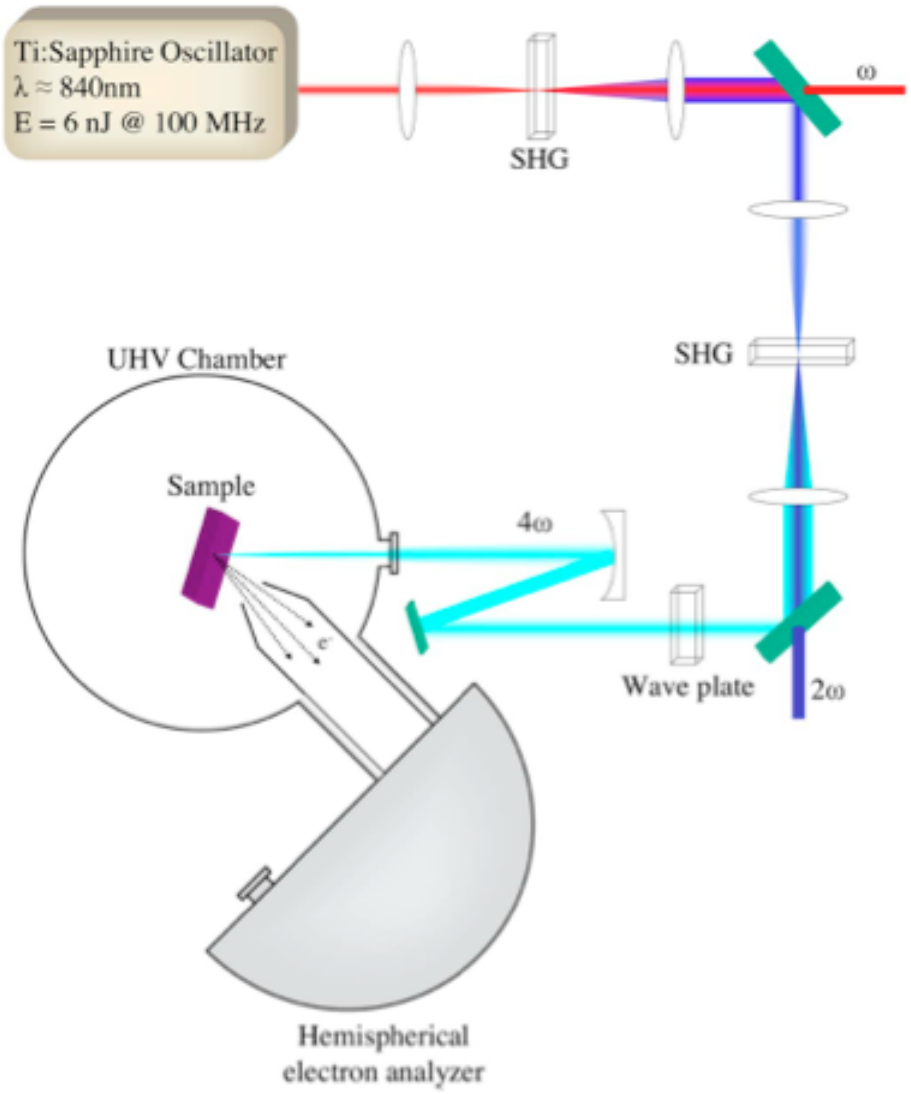

Figure 1.1: Schematic Layout of the Dessau Group ARPES System [11].

frequency ω_0. Additionally, Einstein proved that:

$$K_{max} = \frac{1}{2} m_e v_{max}^2 = q_e V \tag{1.2}$$

where m_e is the mass of the electron, v_{max} is the maximum velocity of the photoelectron, q_e is the charge of the electron, and V is the stopping potential. This equation shows that the maximum velocity of the photoelectron is independent of the intensity of light. In essence, a higher intensity leads to more electrons, not higher energy electrons. By conservation of energy we then get the binding energy of the electron as:

$$E = \hbar\omega - K - \phi \tag{1.3}$$

where K is the measured kinetic energy of the photoelectron, and E is the binding energy of the electron. Assuming a smooth scattering surface, translational symmetries require the component of momentum parallel to the direction of the beam to be conserved:

$$\hbar k_{i\parallel} = \hbar k_{f\parallel} = \sqrt{2mK} \sin\theta \tag{1.4}$$

where $\hbar k_{i,f\parallel}$ are the initial and final components of the momentum parallel to the plane of the sample respectively. However, the component of the momentum perpendicular to the plane of the sample is not necessarily conserved:

$$\hbar k_{i\perp} = \sqrt{2m(K\cos^2\theta + V_0)} \tag{1.5}$$

where $\hbar k_{i\perp}$ is the initial component of the momentum perpendicular to the plane of the sample and $V_0 = |E_0| + \phi$ is the band depth from vacuum (E_0 corresponds to the energy at the bottom of the valence band) [7].

With data on the wave vectors $k_\parallel$ and $k_\perp$, it is then useful to construct what is called a Fermi Surface. Fermi surfaces are plots of the $k_\parallel$ vs. $k_\perp$ vs. Energy graphs that are useful for deriving electric and thermal properties of objects (see Fig. 1.2 and Fig. 1.3). The figures only picture the first Brillouin Zone, which is the area in k-space created by taking planes at the points equidistant to the surrounding lattice points. This structure is periodic so the Brillouin Zone can be transposed periodically to obtain a plethora of information about the material.

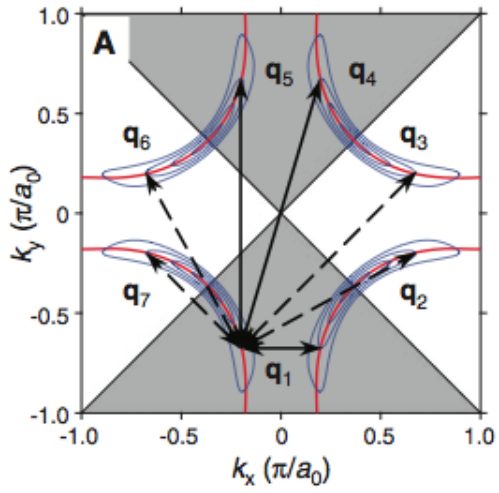

Figure 1.2: Normal-state Fermi surface (red curves) of a High-T_c cuprate, arrows illustrate 8-fold symmetry [8].

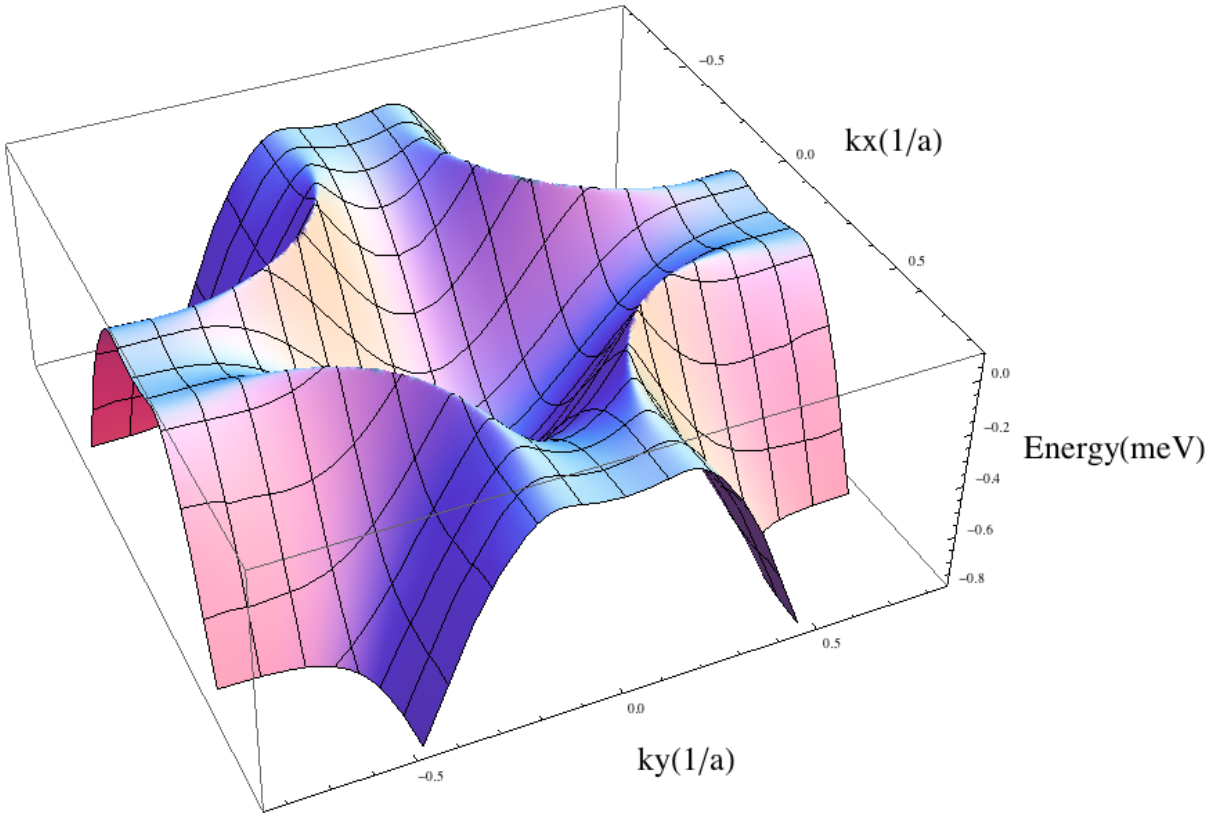

Figure 1.3: A 3D theoretical representation of the Band Structure of BSCCO with $k_{||}$ and $k_{\perp}$ on the x- and y-axes and electron energy on the z-axis. Courtesy of Matthew Kilpatrick.

1.4 Advantages

This UV Light Source has many advantages over the current 7 eV Titanium-Sapphire laser in place at the Dessau Group. On an elementary level, this UV Light Source is capable of producing photons with a higher energy than 7 eV. Higher photon energy is valuable because higher energy photons lead to higher photoelectron velocities (Eq. 1.2). Ambient magnetic fields are a major source of error in ARPES, which is the reason why the Dessau group's ARPES system is made primarily out of magnetic field damping μ-metal, but even so, ambient magnetic fields still cause some electrons to deflect enough to be registered as noise instead of signal [11]. Higher photoelectron velocities will reduce the deflection caused by these ambient magnetic fields.

While a photon energy increase from 7 eV to 9 eV (for Argon) may seem nominal at first glance, one must factor in the work function of the material (Eq. 1.1). As an example, the work function of BSCCO is $\sim$5 eV. This means that the maximum kinetic energy of photoelectrons using the current 7 eV Titanium-Sapphire laser is $\sim$2 eV. With 2 $\frac{\text{eV}}{\text{c}}$ of momentum available to distribute over $k_{\|}$ and $k_{\perp}$, only a portion of the first Brillouin Zone is accessible, a portion that is notably excluding a region of particular interest on the Fermi Surface known as the anti-node. Thus an increase in incident photon energy by 2 eV actually amounts to a 100% increase in the visible area of the Fermi Surface, allowing access to all of the first Brillouin Zone.

Advantages of higher photon energy are not simply based on the magnitude of the photon energy; it is an optimization of photon energies. The Dessau Group often visits synchrotrons throughout the world and uses photons with energies much higher than 9 eV to examine High-T_c superconductors. During these visits, the group determined that lower energies are not only a more precise means of examining these materials, but sample lifetime is drastically reduced by high energy photon bombardment. Thereby, 9 eV light optimizes the ability to view all of the first Brillouin Zone with the sample lifetime in order to maximize the Dessau Group's data output, in terms of both quantity and quality of data.

The advantages of a CW mode light source over a PW mode light source can be found by

examining the mechanism of the photoelectric effect. When electrons are scattered off of a material by PW light, if the frequency of the pulse is short and the number of incident photons large, the electrons will see an enhanced space charge effect, which negatively affects energy resolution. Alternatively, light in CW mode scatters electrons continuously off of the surface, allowing for a more continuous spectrum.

Perhaps the largest advantage this UV Light Source provides is versatility. There are many different photon energies obtainable by using noble gases and gas combinations, some with very narrow bandwidths (see Table 2.1). Even those photon energies with wide bandwidths can be monochromatized (see Section 2.7), meaning many possible wavelengths are capable of being harnessed by this system.

Chapter 2

The Novel High-Brightness EUV/VUV Excimer Light Source

2.1 Schematic Representation

As previously stated and illustrated in Figure 2.1, the UV Light Source consists of an electron gun, which is only operable in Ultra-High Vacuum (UHV, 10^{-8} torr), which is incident on a diamond barrier that holds vacuum against a chamber with a high density of noble gas. The electrons are transmitted through the barrier and incident on the nobel gas to form excimers that quickly decay, emitting UV light. This UV light is then harnessed and directed into an ARPES chamber.

This section will describe the setup of this UV Light Source in full by examining this system by its individual components in full detail to see exactly how this machine functions.

2.2 Electron Generation

For generating electrons we are using a Kimball EMG-4210/EGPS-4210 Electron Gun and Power Supply System coupled with a VSW X-Ray high-voltage (HV) Supply.

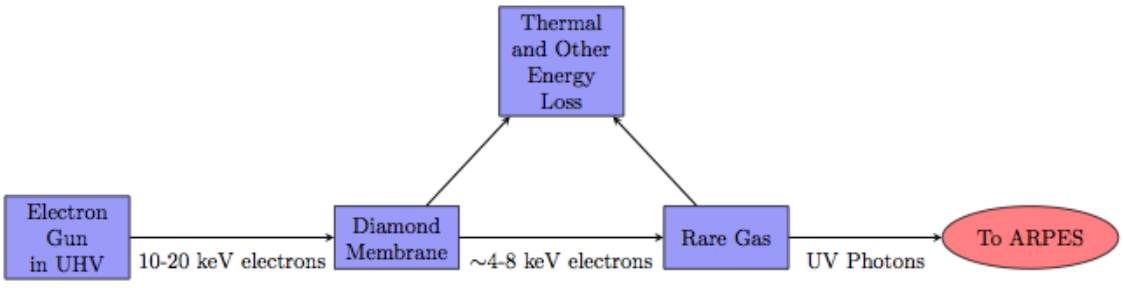

Figure 2.1: Flow chart illustrating the UV Light Source setup.

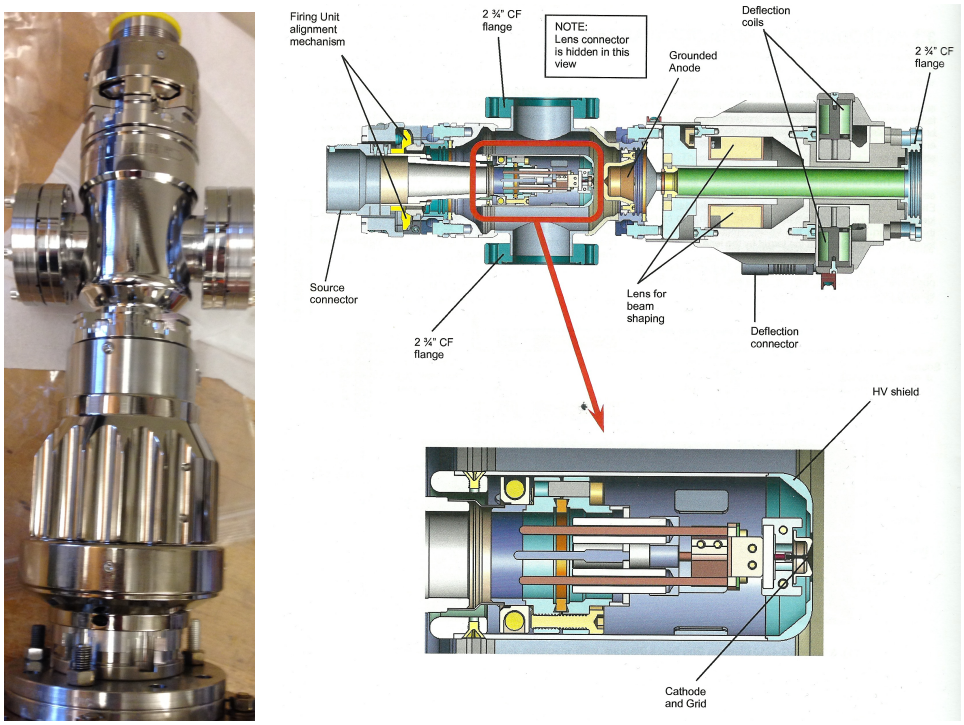

Figure 2.2: Kimball Physics EMG-4210 Electron Gun (left) and Schematic [10] (right).

The EMG-4210 (see Figure 2.2) Electron Gun is capable of generating a gaussian beam of 1-30 keV electrons with a current of 0.01-20 mA. The spot size ranges from 0.1-100 mm dependent on the working distance (0.05-1 m). The cathode in this electron gun is a LaB_6 emitter which is heated by a voltage between 0-30 kV (limited by the VSW HV Supply). The electrons are then focused and shaped by beam shaping coils [10]. Emission current is a function of both temperature and emission energy. At high energy and low temperature (temperature-limited region), current (J) goes as:

$$J = AT^2 e^{\frac{-\phi}{\kappa * T}} \tag{2.1}$$

where J is the emission current ($\frac{A}{cm^2}$), T is cathode temperature (K), ϕ is the work function of the cathode material (eV) , κ is Boltzmann's constant ($8.6 * 10^{-5}$ $\frac{eV}{K}$) and A is Richardson's constant for LaB_6 = 120 $\frac{A*K^2}{cm^2}$ [10]. At high temperature and low energy (space charge-limited region) J goes as:

$$J = 2.335 * 10^{-6} * \frac{V^{\frac{3}{2}}}{d^2} \tag{2.2}$$

where V is the high energy potential applied to the cathode (V) and d is the distance between the anode and the cathode (cm) [10]. It is important to examine these equations to determine what current we can expect through the diamond membrane, as well as in which regime we are operating. This operational regime is indeterminate for the time being (as we have not yet tested electron transmission) but it will become important for the characterization of the system.

The VSW X-Ray High-Voltage (HV) Power Supply limits our system in that the voltage source is at a maximum ∼16.5 kV. This means that we will only be able to access a limited amount of intensity, as the HV source will not be able to fully heat the cathode, meaning fewer electrons will boil off. However, all other components are controlled by an independent voltage source provided by the EGPS-4210 Power Supply System. Additionally, the HV Supply has a large, 60 Hz 200 V peak-to-peak ripple, so when we view the light produced on a phosphor screen, we should be able to see a periodic light intensity oscillating at 60 Hz. While this HV Power Supply is unsatisfactory for use in an ARPES application, the VSW HV Supply should more than suffice for these preliminary proof-of-concept tests. The actual UV Light source will need to be adjusted in many facets before being implemented in ARPES, which will be discussed throughout this chapter.

2.3 Diamond Membrane

The Diamond Window (Figure 2.3) is the most integral, novel part of this whole apparatus. As such, the bulk of the work in this project went into finding a suitable method of making and implementing this diamond window, and in a sense, the entire machine is designed around it. The choice of diamond as the window between vacuum and noble gas is, as previously stated, due to diamond's unique combination of high thermal conductivity and low electrical conductivity. This section will discuss in detail the process of manufacturing, preparing, and implementing the diamond membrane as the window between vacuum and noble gas, beginning by classifying the type of diamond used as the window.

Figure 2.3: A photo of the diamond membrane on the silicon frame. The orange tape is for keeping track of the alignment corner

2.3.1 Types of Chemical Vapor Deposition Diamond

Chemical Vapor Deposition (CVD) Diamond is a process in which a heated hydrocarbon gas (typically methane) is used to grow diamond from a substrate or diamond seed. Methods for growing diamond vary, and the properties of different types of CVD diamond vary dramatically as well.

While the properties of CVD diamond vary with the environment in which they are made, there are four classifications of CVD Diamond: Single-Crystal, Micro-Crystalline, Nano-Crystalline, and Ultranano-Crystalline (scD, mcD, ncD, and uncD respectively) [3, 19]. These structures differ in the size of the coherent diamond crystals (grains). scD contains a single coherent diamond grown from a single diamond crystal grain substrate, whereas mcD , ncD, and uncD are polycrystalline diamond films made of grains on the order of $\sim$1 μm, 10-100 nm, and $<$10 nm respectively, typically grown from non-diamond substrates [19]. For this UV Light Source we will use ncD due to accessibility, which poses unique problems owing to the incoherence of ncD crystalline structure.

While diamond is the hardest material on the Mohs Hardness scale (and ncD is actually harder than diamond), we will be using 0.5 μm and 0.3 μm thick diamond membranes for our

windows. This means that our window is very weak to forces normal to the plane of the window and susceptible to breaking. Thus, an extraordinary amount of care and consideration must be taken when fabricating and handling these windows so as to not break them.

2.3.2 Burst Pressure

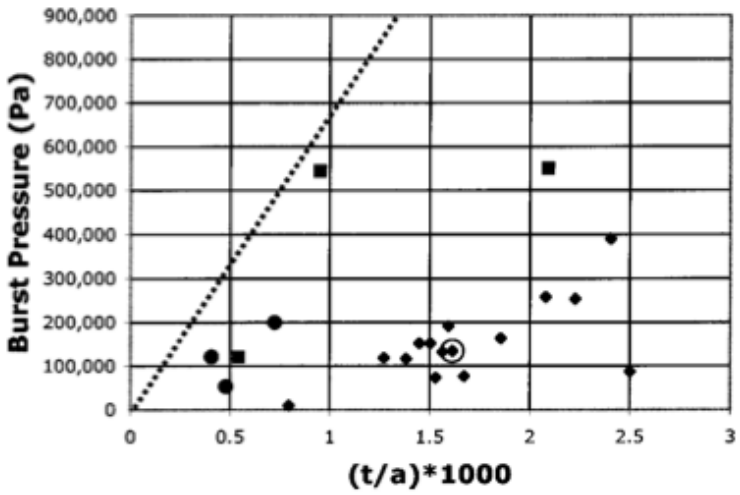

Figure 2.4: Burst pressure vs. $1000 * \frac{\text{membrane thickness}}{\text{membrane radius}}$. Solid circles indicate ncD films and the dotted line indicates natural scD burst pressure [19].

This breaking due to normal force poses the largest challenge to this experiment, in that the diamond window will be used to hold up to an atmosphere of gas against vacuum. Figure 2.4 shows the burst pressure of diamond vs. $1000 * \frac{\text{membrane thickness}}{\text{membrane radius}}$. Keeping in mind 1 atm = 101,325 Pa, we can see that ncD thickness/radius ratios of $\sim$0.5 are capable of holding a vacuum against atmosphere but are not necessarily guaranteed to do so. With this knowledge, we will use a .5 μm thick window with an unsupported, exposed circle of diamond with a diameter of .0235" (.5969 mm) for proof-of-concept. Thus, thickness-radius ratio is $\sim$1.6, clearly above the threshold that holds atmosphere for ncD. This membrane geometry will also work with our electron gun, considering it is capable of focusing down to a spot size of 0.1 mm (page 11). There is, however, a caveat to looking at Figure 2.4 in that none of the data points used diamond membranes as thin as 300 nm—most were on the order of 1 μm [19]—and as such, 1.6 is a conservative thickness-radius ratio,

considering our supply of diamond windows is limited.

2.3.3 Manufacturing the Diamond Windows

Manufacturing the diamond membrane proved to be the most time-consuming aspect of this project. As shown in Figure 2.5, the thin film diamond is deposited on a silicon substrate. In order to expose only diamond, the silicon substrate must be etched down in the precise spot where exposure is desired.

This process proved to be time consuming due to the lack of resiliency of the diamond and the impurity of the masking agent we had available. Initially, we tried to etch the silicon using an anisotropic KOH etch (which etches in the 110-plane of Si) after using lithography (explained in Section 2.3.4) to mask the Si with Silicon Nitride (SiN). The etch rate of Si in KOH is dependent upon the temperature of the bath, and we quickly found that neither the diamond nor the SiN could withstand a fast etch rate. Unfortunately, we determined that SiN of the purity we had available at the Colorado Nanofabrication Laboratory (CNL) was not suitable to mask the Si for the time it would take to etch through the 500 μm of Si on which the pictured diamond is deposited. Additionally, the diamond developed fractures owing to KOH leakage through the ncD that etched the silicon in an undesired direction, presumably originating at holes between diamond grains (see Figure 2.6). Thus, effectively executing this process would require not only masking the Si side, but the ncD side as well. As such, to execute this process to the desired precision would take approximately 100 hours to produce a single exposed diamond membrane (60+ hours of masking both the diamond and Si sides with SiN, 40+ hours of etching), and because CNL charges by the hour, this procedure quickly became cost-ineffective.

Following this realization, we reached out to Dr. Bradford Pate, a research physicist and head of the diamond materials group at the Naval Research Laboratory, with whom Professor Dessau is acquainted. Dr. Pate provided our group with 9 separate samples of exposed $\sim$3 mm diameter ncD membranes on 1 cm x 1 cm Si substrates (Figure 2.3) with 4 of those samples being 300 nm thick ncD and 5 being 500 nm thick ncD. These windows were exposed using a specialized system

Figure 2.5: The diamond side of 0.3 μm thick diamond film deposited on a 500 μm thick Si substrate

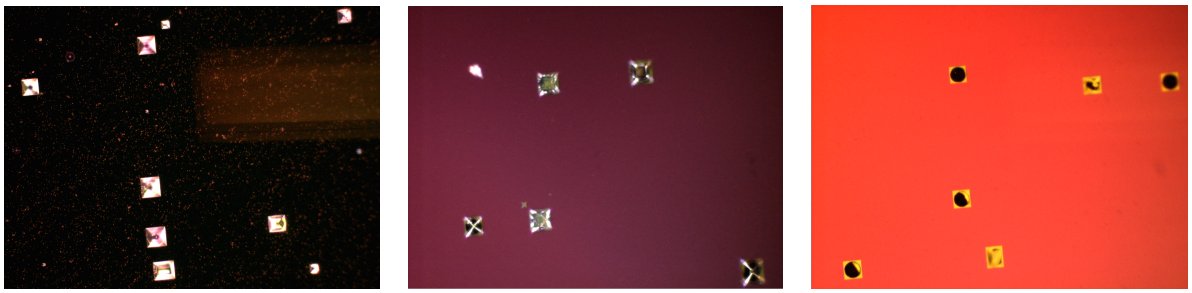

Figure 2.6: Three different polarizations of KOH-diamond fracturing with a x100 microscope. Note the square shape of the fractures indicating the KOH has isotropically etched the Si beneath the diamond in the 110-plane.

that involves flowing nitric acid over the Si to convert the Si to Silicon Oxide (SiO_2) then dripping HF acid on the surface in the desired location. The nitric acid is sucked away once it etches the SiO_2 down to the Si. They repeat this process until the Si is etched completely away and only diamond remains. The HF drip location is not mechanically centered on the Si chip, and as such the diamond windows in each of these are slightly off-center, a fact that must be considered when designing the copper piece onto which the diamond will be soldered into place.

2.3.4 Preparations For Soldering

Preparing the diamond so that it is capable of being soldered into place on the copper window holder described in the following section presents another challenge. There are two main goals when it comes to soldering the diamond: creating as much of a support structure as possible for the exposed membrane and providing the best possible thermal contact to the copper window holder. In order to accomplish these goal,s, we used a Chemical Vapor Condensation (CVC) machine (Figure 2.7) to evaporate a thin layer of chromium (15 nm) then a thin layer of gold (30 nm) on top of the diamond. The CVC works by running current through the desired metal in a vacuum ($\sim 2 * 10^{-6}$ Torr) that causes those metals to evaporate. Suspended above the metal is a rotating chuck which holds the sample. Additionally, a metal shadow plate mechanically swings in front of the sample holder, so that a user can accurately control the amount of evaporated metal incident on the sample. When the shadow is in front of the sample, the shadow is 0.7" away from the sample.

Figure 2.7: Photo of the CVC machine at CNL

This process has its own set of complications. The most accurate masks are created by lithography, which requires spinning photoresist onto the desired face, exposing that face to UV

light through a mask, developing the mask, evaporating the metals onto the face, then etching the photoresist away to leave metals in only the desired location. Spinning photoresist requires putting the sample onto a rotating vacuum disk, which would surely break the fragile membrane (thickness/radius ratio >> 0.5). Applying liquid photoresist onto the surface of the diamond might break the membrane as well.

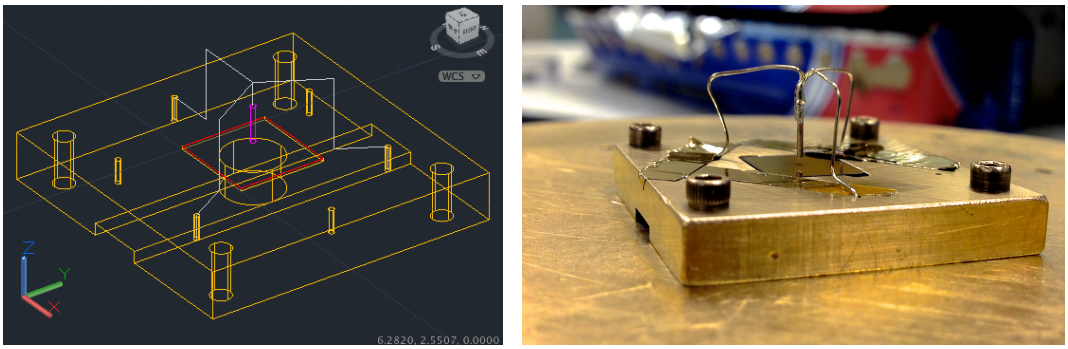

Figure 2.8: (left) An AutoCAD rendering of the mechanical mask and (right) the mechanical mask and diamond chip following Cr-Au deposition.

To avoid breaking the membrane we designed a mechanical mask that fits into a brass holder (see Figure 2.8). The brass holder consists of a brass base with a 0.010" deep divot for holding the diamond wafer. While milling the corners of this divot, we overshot the wall in order to ensure flat corners. Additionally there are four 2-56 bolt holes to insure the wafer is fastened into the center of the sample holder. In order to hold the diamond in place (as it sits upside-down in the CVC), we used specialized evaporator tape. This tape was prepared such that most of it would be sticky, but a small piece is cut and placed sticky side against sticky side. We then position this feature to hold the diamond wafer in place such that no sticky part sticks to the diamond. This consideration is made lest the removal of the tape from the diamond breaks the membrane.

There is a .25" hole drilled through the center of the aforementioned divot and a channel milled out of the underside of the brass holder. This is a consideration again in order to not break the diamond. When the CVC goes under vacuum this channel and hole ensure no air is trapped in between the brass and the diamond membrane—called a virtual leak—most likely breaking the

diamond membrane. This channel allows us to evacuate beneath the diamond membrane and ensure no virtual leaks.

The wireframe mask consists of a malleable wireframe structure that rises from the brass holder 0.3". Because the brass holder is 0.2" thick, the wireframe structure fits well under the shadow in the CVC. The wire support is then soldered to a AWG 22 wire which is 0.0253" in diameter, which is soldered into a position ∼0.05" above the diamond sample. This process is used owing to concerns about breaking the diamond window. There is also a hexagonal bolt pattern of holes with a diameter of 0.0235" for holding the wireframe in place, a bolt that is taped down during evaporation. As can be seen in Figure 2.9, this 0.05" separation caused a fuzzy circle of evaporated Cr-Au around the exposed diamond membrane, whereas lithography would result in a much cleaner mask with no fuzziness.

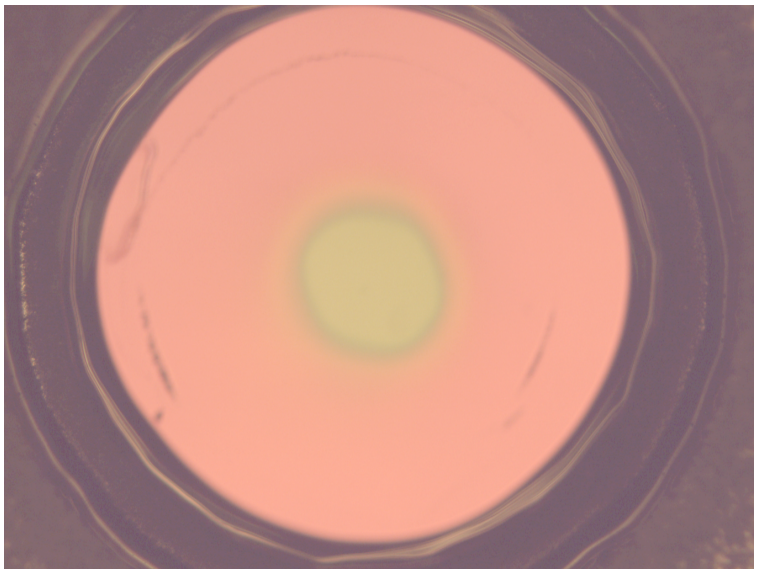

Figure 2.9: A x30 Microscope photograph of the diamond membrane following evaporation. Green indicates exposed 0.5 μm diamond, red indicates evaporated Cr-Au, and grey indicates Si.

A very strange phenomenon occurs shown in Figure 2.10 where the edge of the diamond chip is burnt following the evaporation. This burning might pose a problem if it is raised from the plane of the deposited gold. By examining the thin film interference (the rainbow pattern between the burnt edge and the gold), we are able to determine whether this burning is raised with respect to the

gold plane or sunken. Referring back to Figure 2.5 we see the same thin film interference pattern. Knowing that the diamond wafer increases thickness between the edges and the center, we can see that increasing thickness on thin film interference patterns periodically goes from blue to green to red. Applying that insight to Figure 2.10, we can see that the thickness of the burnt material increases as it moves towards the edges (bottom of photo). This burnt area is lost thermal contact. Fortunately, this area will not be seeing any thermal load; the affected area is very small, and the burnt area is only raised from the plane of the Cr-Au by ∼2 wavelengths of light by inspection of the thin film diffraction, so it should not pose a problem, though it is worth noting.

Figure 2.10: Microscope photograph of edge of diamond following deposition. Note the black burning and rainbow thin film interference bleeding into the deposited gold.

2.4 Window Holder Ensemble

The window holder ensemble consists of a copper window frame (red in Figure 2.11) and a thermal isolation conflat (grey). This section describes the rationale behind the shapes of each of these elements. The subsequent section describes the pictured cooling attachment (cyan and green) and the rest of the cooling system.

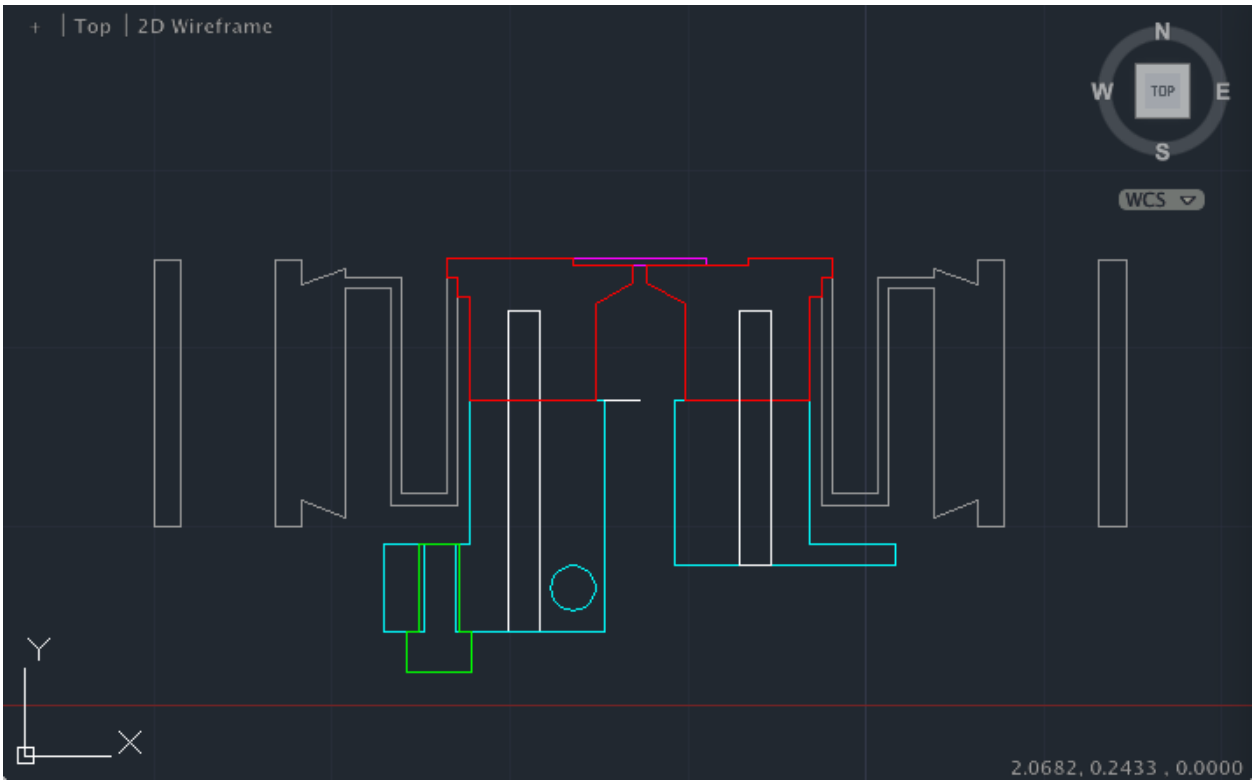

Figure 2.11: A cross section of the thermal isolation conflat (grey), the copper window frame (red), and the copper cooling attachment (cyan) and thermometry (green). Diamond membrane is shown in purple

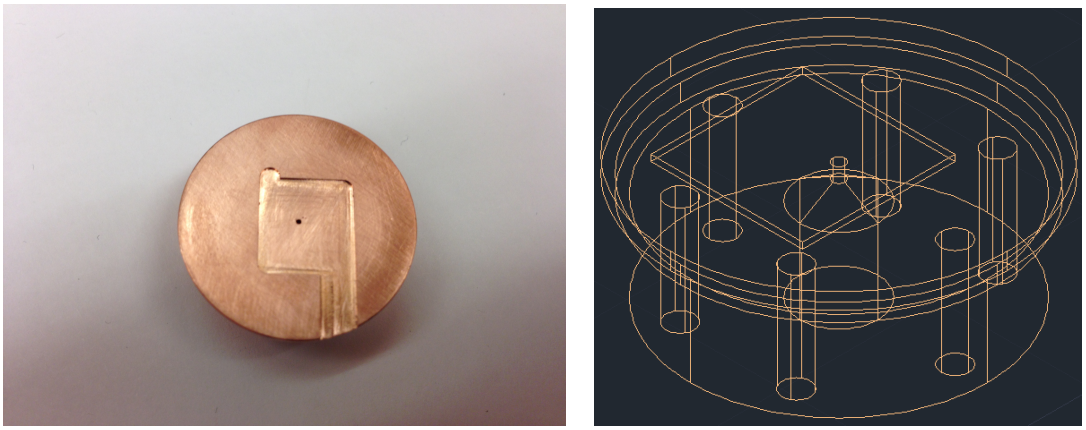

Figure 2.12: A photo detailing the facial divot where the diamond membrane will be soldered (left) and an AutoCAD schematic of the copper window frame (right)

2.4.1 Copper Window Frame

The copper window frame (Figure 2.12) has a divot much like the divot in the brass holder (Figure 2.8), but the design of this divot is oversize and off-center such that we can position the alignment corner of the chip (illustrated in Figure 2.3) against the upper left corner of the divot. By aligning like as such, the exposed diamond membrane is positioned exactly above the 0.0235" diameter aperture drilled into the copper frame, which is drilled into the center of the frame. The reason for this alignment process is the inexact nature of the Si etching process described in Section 2.3.3 (page 15). Thus, we must mill out the divot off-center so that the diamond membrane perfectly aligns with the center of the window frame. Additionally, this divot is oversize so that the solder we use to secure the diamond window to the copper frame does not bead up around the walls and corners of the divot, knocking our diamond membrane out of alignment.

As pictured, there is also a step milled around the edge of the copper window frame. This step feature is included for the purpose of interlocking with the Thermal Isolation Conflat (described in the next subsection) with a small area of contact. This insures minimal thermal conductivity between the copper window frame and the stainless flange, as elaborated upon in the following subsection.

Additionally, there is a hexagonal bolt hole pattern of threaded 4-40 holes for fastening the

copper cooling attachment to the copper window frame in an attempt to maximize thermal conductivity, while also not soldering the cooling attachment to the frame (for reasons of convenience and versatility). The bolts that secure the copper cooling attachment (cyan) to the copper are vented (they have one side of their threads ground down) such that we are able to evacuate the blind tapped holes in the copper window frame, ensuring no virtual leaks. This process will be used for all blind tapped holes in vacuum.

2.4.2 Soldering the Diamond Membrane to the Copper Window Frame

To solder the diamond membrane onto the copper window frame, we first use flux to burn all of the oxides off the divot in the copper window frame, such that the solder may wick completely over the copper surface and eliminate virtual leaks. Indium solder is chosen for its thermal conductivity, and once the flux is burnt off of the divot, we apply the indium to the divot and spread it down in an even layer. Following this, we thoroughly wash the copper piece, as any remaining flux will negatively affect our vacuum quality. Then we position the diamond membrane so that the alignment corner (as illustrated by the orange triangle in Figure 2.3) is flush with the upper left wall (as seen in Figure 2.12) and heat up the copper window frame, until the solder melts, bonding the diamond membrane to its correct location on the copper window frame. We then let it cool and wipe it clean with ethanol, carefully avoiding the fragile diamond membrane before fastening it into its proper location in the system (see Figure 2.18).

2.4.3 Thermal Isolation Conflat

The thermal isolation conflat (Figure 2.13) is designed to interlock into the copper window frame such that the copper window frame is thermally isolated from the rest of the system, as pictured in Figure 2.11. Thermal isolation is accomplished by minimizing the thermal contact area and maximizing thermal path length. The area of contact between the thermal isolation conflat and the copper window frame = 0.212 in^2 whereas the soldered area between the two = 0.107 in^2. The thermal isolation conflat flange is designed such that the heat from the copper must travel down a

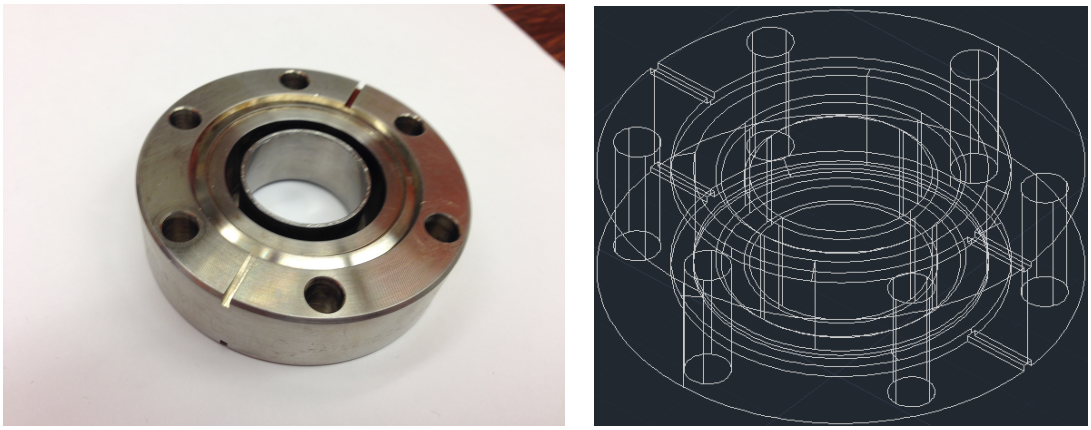

Figure 2.13: A photo (left) and AutoCAD rendering (right) of the Thermal Isolation Conflat

long, thin length before reaching the rest of the outside system. However, this flange design may be neither long nor thin enough to effectively isolate the system, which is a possibility discussed in the following section.

2.5 Cooling and Thermometry

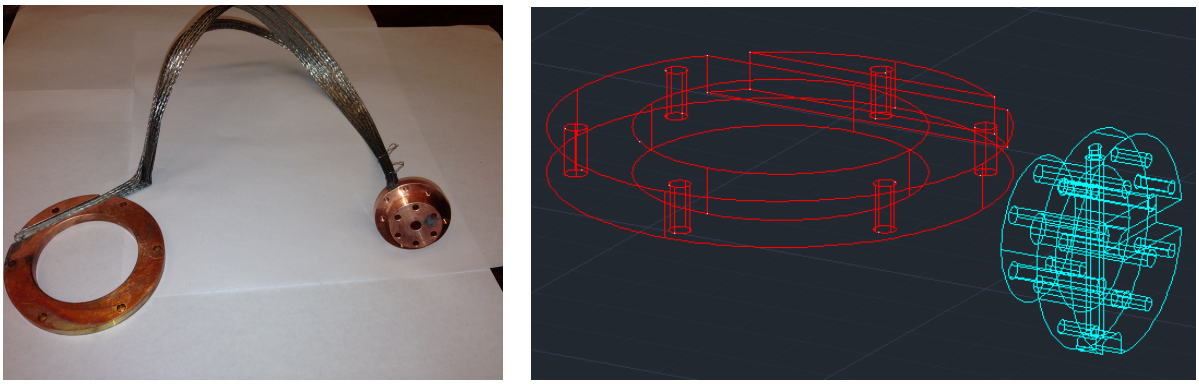

Figure 2.14: A photo (left) and AutoCAD rendering (right) of the cooling attachment and gasket. Cooling braid attached in photo.

The cooling system is a CTI Cryodyne Two-Stage Refrigerator pumped by a CTI Compressor, both full of 99.999% Pure He gas. The second stage of this cooling system cools to < 10 K temperatures; however, the diamond membrane is being cooled in order to suck out as much heat as possible. Therefore, our cooling apparatus attaches to the second stage of the refrigerator in

order to conduct away the thermal load. Whereas the maximum thermal load of the second stage is 6 W, the maximum thermal load on the first stage is 25 W, thus the first stage is much more effective at sucking away the thermal load deposited by the electron flux. There is also a copper top attached to the refrigerator and the cooling gasket (red in Figure 2.14) to shield the refrigerator from radiative loss, as well as serve as a support structure to prevent the cooling braid from touching the walls of the system (see Figure 2.15).

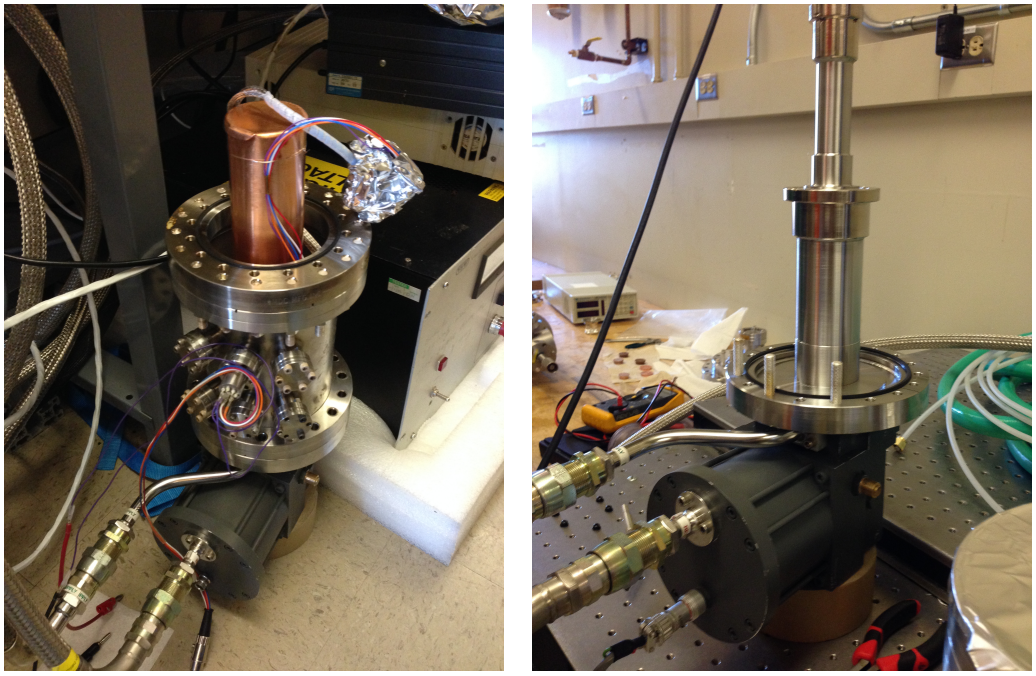

Figure 2.15: A photograph of the CTI Two-Stage Refrigerator with (left) and without (right) the copper top attached and thermometry.

The first stage cools to a temperature of 40 K with no thermal load. If the thermal isolation conflat does not provide adequate thermal isolation from the rest of the system, or if the cooling braid touches a wall, our system will ice over on the outside—starting from around the thermal isolation conflat or point of contact and propagating around the whole system. This is disadvantageous in terms of safety and convenience. Consequently, any potential cooling braid contact points will be insulated with teflon and we have installed a resistive heating element inside the cooling attachment (cyan in Figure 2.14, the heating element is located in the hole that runs vertically as

pictured).

With this heating element as well as a diode thermometer, we control the temperature of the diamond membrane with a LakeShore 330 Autotuning Temperature Controller. With this temperature controller, we will set the temperature of the diamond membrane to 120 K. This temperature is chosen because the thermal conductivity of diamond is at a maximum of 5450 $W/(m \cdot K)$ at a temperature of 120 K [14]. This will insure that the thermal load deposited upon the diamond will be removed as quickly as possible, while simultaneously preventing icing around the thermal isolation conflat.

The diode thermometer must be calibrated to a three-point temperature curve prior to being inserted into the chamber. The three points on this temperature curve are liquid He (4 K), liquid N (77.35 K), and room temperature ($\sim$300 K). This will ensure an accurate temperature reading of our diamond membrane.

2.6 Vacuum Pumping

For the bulk of this system, we will be using stainless steel conflats with Viton gaskets, although some Kwik Flange (KF) will be used to secure the vacuum line to the turbo (for convenience) and some copper gaskets will be used in place of Viton gaskets to insure vacuum is held around particularly large conflats. Conflats used in tandem with Viton and KF are both capable of holding vacuum up to 10^{-8} torr. While the use of conflats in tandem with copper gaskets holds vacuum better ($> 10^{-11}$ torr), this system is taken apart and put back together many times, and copper is economically inefficient because it cannot be reused. Copper is not reusable because when it is fastened between two conflats, the knife edge of the conflats cuts into the copper on both sides to ensure a seal, whereas the knife edge simply pinches the Viton to form a seal. Therefore, when tightening around a copper gasket, procedural care must be taken to ensure the knife edge cuts into the copper with even pressure all the way around the gasket. If this care not taken, the system will leak. The permanent system that we hope to develop for ARPES following this study will exclusively feature copper gaskets.

Figure 2.16: A photo of the Pfeiffer Turbo vacuum pump used for this project

For this system we will be using a Pfeiffer Turbo vacuum pump (see Figure 2.16) to pump whatever must be under vacuum down to the necessary pressure. Because the electron gun does not operate above 10^{-7} torr, we will need to pump out to below this pressure. Preferably, we would like to pump down to pressures as low as possible, as the filament lifetime of the electron gun is reduced by a poor vacuum [10]. The Pfeiffer Turbo is capable of reaching pressures $> 10^{-11}$ torr with a bakeout—a process that heats the chamber to boil off any atmospheric gases stuck to the walls. However, a bakeout is not necessary if the chamber is adequately clean.

Cleanliness in terms of UHV means having a vacuum chamber that contains only materials with low outgassing. Outgassing is the release of gas trapped inside materials that negatively affects vacuum quality. Oils tend to outgas more than most substances, thus utmost care is taken with this system to ensure the vacuum chamber is completely devoid of oil. This means all of the

vacuum chamber parts (excluding the electron gun, which is already UHV ready and refrigerator, which is too big) are first cleaned by hand, then cleaned in an ultrasonic bath. Following the sonic cleaning, these parts (including the refrigerator) are wiped down with Acetone, then Isopropanol, then Methanol (AIM). Additionally, only UHV suitable solders (silver) and tapes (Kapton) are used in vacuum.

2.7 Optics

This section outlines some basic properties of Ultraviolet light and excimer decay as well as optical elements that will be used in the permanent version of this UV Light Source.

2.7.1 Ultraviolet Light

Vacuum (VUV) and extreme ultraviolet (EUV) light are distinct from other forms of UV light due to their absorption. VUV has wavelengths in the range 10-200 nm whereas EUV has wavelengths between 10-121 nm [21]. As "vacuum" implies, VUV and EUV are most easily manipulated in vacuum. This is due to their strong absorption by atmospheric oxygen. However, some industrial applications for VUV use pure nitrogen environments because N_2 is transparent to VUV in the range 150-200 nm, which is important in terms of system design for Deep UV Photolithography processes and other potential applications (Section 4.3).

2.7.2 Excimers

The eximer decay transition occurs in a chamber (Figure 2.17) bolted to the Thermal Isolation Conflat, which features a filament probe for measuring current as well as a means of pumping the chamber both to vacuum and to an atmosphere of Noble Gas.

Excimer decay occurs via many different excitation and relaxation paths (as described for xenon in [12]), but the process always takes in high energy electrons and produces UV light. The wavelength of this UV light is dependent upon the species of gas(es) (as described in Table 2.1), whereas the intensity is dependent upon the electron flux incident on the gas. In gaseous mixtures,

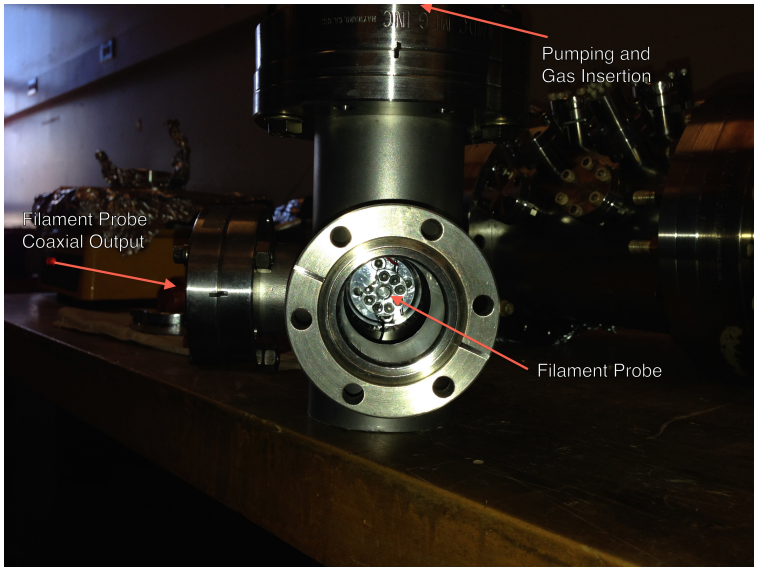

Figure 2.17: A photo of the excimer decay chamber with the Filament Probe attached

the excimer photon emissions tend to have a much narrower bandwidth than in their pure gas counterparts. This will be a useful tool for ARPES, as the Ar/O_2 gas mixture may be advantageous over pure Ar in that it has a narrow bandwidth, and the light would not need to be monochromatized to be harnessed for ARPES (as long as it emits in a single, narrow peak).

Table 2.1: Rare Gas Photoemission Wavelength, Energy, and Bandwidth [15]

Gas or Mixture	Average Wavelength (nm)	Average Energy (eV)	Emission Bandwidth (nm)
He	60/80	20.7/15.5	20
Ne	83	14.9	4.5
Ar	**126**	**9.8**	**9**
Kr	147	8.4	11
Xe	172	7.2	14
Ar/Xe & Kr/Xe	147	8.4	< 0.1
Ar/O_2	130	9.5	< 0.1
Ne/Ar/Kr	124	10.0	< 0.1

Argon data in bold for reference; note narrow bandwidth of gas mixtures.

The filament probe will be useful for characterizing the electron transmission through the diamond membrane (Chapter 4) as well as for the characterization of the mean free path of electrons in Argon (Chapter 5), whereas it will be removed and replaced with a phosphor screen for the proof

of concept. The filament probe is simply a wire that is able to move towards and away from the diamond membrane inside of the excimer decay chamber. It is capable of extending 2", and with it we can get as close as 300 μm away from the diamond window (the thickness of the silicon frame of the diamond window).

This filament probe will be positively biased (meaning we will run a positive DC current through it then resolve that offset in the data) so as to attract all electrons from the electron gun while simultaneously repelling the positive ions floating around inside the excimer decay chamber while testing the mean free path of electrons (see Section 3.3). Whenever the filament probe is used, the electron flux used will not be large enough to generate light, even in the case of measuring the electron mean free path. This will be done so as to prevent the filament from emitting photoelectrons (as described in Section 1.3) which would then be absorbed by the positively biased filament. Additionally, current large enough to generate light would require cooling considerations on the filament probe.

2.7.3 Optical Elements

While the extent to which we will use optics is limited in this project, a discussion of the optics used in EUV/VUV applications will allow a basic understanding of the properties of the optical elements this UV Light Source will contain when set up permanently.

Lithium Fluoride (LiF) transmits light of wavelengths in the range 0.12 to 6 μm [13]; while they have a myriad of characteristics that make them tough to work with—they are very soft and prone to developing color centers (optical defects)—they are the only optical material that transmits light in the EUV/VUV range. Thus, our permanent system will exclusively use LiF optical elements for EUV/VUV light manipulation. Additionally, as discussed in Section 2.7.1, EUV/VUV is strongly absorbed by components of the atmosphere (particularly O_2) and as such LiF optics must be surrounded by either the excimer gas, vacuum, or another gas that does not absorb EUV/VUV. See Section 4.2 for further discussion.

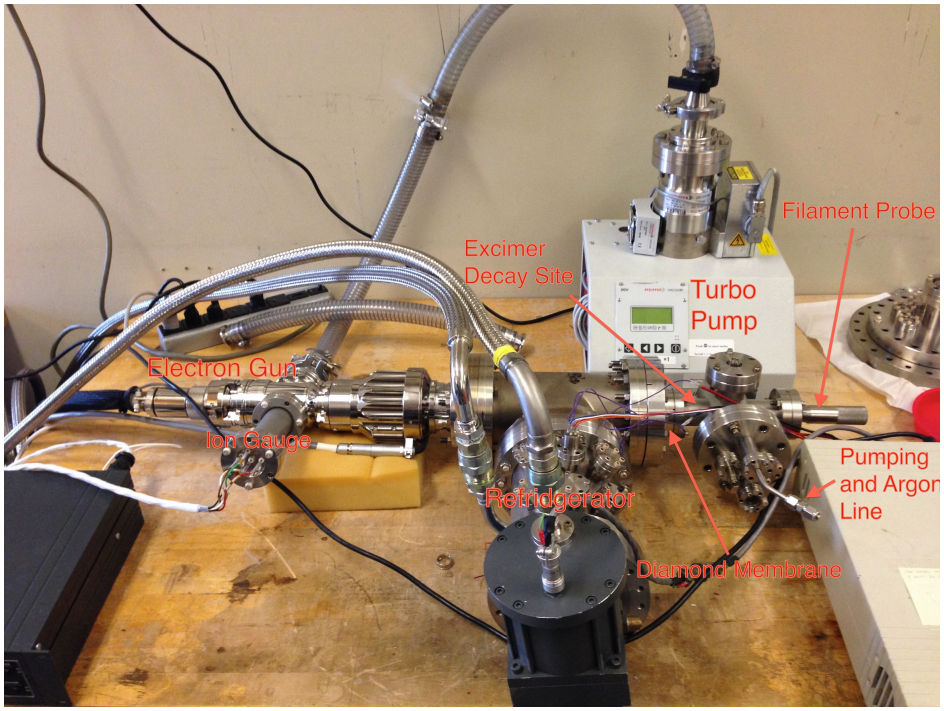

Figure 2.18: A photo of the whole UV Light Source setup

Figure 2.19: A photo of the control systems for the UV Light Source

Chapter 3

Proof Of Concept and Characterizing Tests

The goal for this project is to show that we can use a diamond membrane to generate a fully CW-operable High Brightness EUV/VUV Light. For a proof of concept we must show that the 0.5 μm diamond membrane can hold vacuum from an atmosphere and the thermal load deposited on it by the electron gun. We must also generate EUV/VUV light.

To illustrate a proof-of-concept, we must simply operate the light source. The following section will outline the process of operating the UV light source, as well as the tests used to show that the diamond membrane withstood both held vacuum and withstood the thermal load of the electron flux and that EUV/VUV light was generated.

Because this research project is ongoing, none of the following section has been conducted yet. I am currently working on pumping down the system and calibrating the autotuning temperature controller. As such this thesis has no data, but the methods for taking data will be described below.

3.1 Proof of Concept

3.1.1 Basis

A pivotal component of gaining this proof of concept is insuring we have generated EUV/VUV light. We are posed with a unique problem, considering VUV is quickly attenuated by atmosphere, and would be thereby undetectable outside of vacuum. Additionally, many materials are opaque to VUV, which is actually an advantage when determining whether or not we have generated EUV/VUV light. To insure that we have generated EUV/VUV, we will need to run two separate

operations, completely reseting. This is convenient, as our system must be able to withstand resetting if it is at all useful, and this will serve as a repeatability test.

For the first of these tests, the filament probe will be replaced with a glass viewport. On the gas side of this viewport, we will paint on phosphor paint. Phosphor glows in the visible spectrum when exposed to UV, and we will be able to see this glowing and note at what electron energy and current it begins glowing at, showing that UV light has been generated. After venting the system, we will replace the phosphor painted glass viewport with a glass viewport free of anything. Glass is opaque to VUV, and as we repeat the operation procedure, we should not see any light out of it. If we see light when the phosphor painted viewport is attached and do not when it is not, we can conclusively say we have generated UV. Due to the fact that, with the exception of some Ar impurity (which we will avoid), VUV is the only light Ar is capable of generating with this system, we have generated VUV.

A more rigorous means of testing this would be to attach the end of this system to a monochromator, and resolve the intensity of light generated at various wavelengths. If this matched the argon spectrum, we could conclude that it is indeed VUV we have generated. When we have a permanent system in place we will monochromate the VUV before it is sent into ARPES, and we will conduct this test at that time. For now, this basic proof of concept will suffice.

3.1.2 Pre-operation

The very first test this system must go through is the pump down. Foremost, the system must be able to maintain pressures $< 10^{-7}$, otherwise the electron gun will not have sufficient vacuum to operate properly. Next we must test the resiliency of the diamond membrane. The excimer decay chamber will be wired to a "T" valve. One side of this valve will lead to a conflat near the refrigerator such that, when this valve is open, both sides of the diamond membrane can be pumped down at the same time. The other valve would lead to a regulator connected to a tank of Ar. To test diamond statistics, we would pump nitrogen into the system until the diamond membrane breaks, but for a proof of concept, we will pump .5 atm (380 torr) pressure of Ar into the

excimer decay chamber. If at any point we lose vacuum we will know that the diamond membrane has burst.

Prior to the operation of the system, the electron gun must be conditioned. First, once $\sim 10^{-8}$ torr pressures are achieved, the electron gun must be conditioned for normal operation. This means first applying high voltage only to condition the anode shields, then applying cathode heating only to outgas the firing unit assembly, then applying both cathode heating and high voltage at the same time to insure gun stability after outgassing.

The next operational test is temperature stability. To test stability, we will turn on the compressor. When the refrigerator is turned on and the temperature controller has stabilized at our desired value of 120 K, if the outside of the system begins icing over surrounding our diamond membrane, we know that our thermal isolation flange is inadequate to thermally isolate our sample from the outside system. In this case, depending upon the severity of the icing, we will note the icing and continue on, use a higher temperature (which reduces the thermal conductivity of the diamond), or find a replacement for the thermal isolation conflat described in Section 2.4.3. Additionally, if any of the walls around the thermal isolation conflat ice up before the area around the diamond membrane, we know that one of the cooling braids is touching the wall, and depending upon the severity, we will either cease operations to rectify this fault or continue on. If we lose vacuum for any reason during this time, the diamond membrane has broken and operation must cease.

3.1.3 Operation

Once all of the tests in the preceding section are accomplished and the phosphor painted viewport is attached, the system will be ready for operation. We will use 10 KeV electrons (the low end of electrons capable of causing excimer decay, after the losses from the diamond membrane are considered) but starting at a very small current (ranges from 10μA to 20 mA), and if we do not generate light by a current around $\sim$500μA, we will iterate up through electron energies. If none of the available electron energies generate light, we will add an Ar pressure .05 atm and repeat the

process, monitoring the ion gauge carefully when we increase the pressure.

We will initially operate this beam in manual pulsed mode such that the thermal load mimics the SiN membrane from the Mühlberger group [15, 16]. This is to ensure that the diamond does not break under the thermal stress. However, we will still monitor the ion gauge very closely throughout this process to ensure the diamond membrane has not broken. If the pressure does rise suddenly, we must quickly shut off the VSW HV supply and the electron gun controller, so as to ensure the longest filament lifetime possible. Between these tests, we will examine the diamond membrane under a microscope to see if any holes or defects have opened up, suggesting that ncD is not an optimal membrane for this use.

When the phosphor painted viewport is switched out for a glass viewport, we will set the current, electron energy, and pressure to the lowest setting that generated VUV in our previous test. We should not see any light from this viewport, and after iterating up through electron currents and seeing no light out of the viewport, we will have proved that we have generated VUV light. Once the concept is proven by these two tests, we will again vent the system and change back to the phosphor painted viewport to test that we are capable of generating CW mode VUV light. This simply means operating the system in CW mode, as opposed to the aforementioned pulsed mode. If we do not lose vacuum and generate VUV, we have proven our system is capable of generating CW EUV/VUV.

3.2 Electron Transmission Characterization

In order to characterize the electron transmission of the diamond membrane, we will again vent the system and attach the filament probe to our excimer decay chamber. We will position our filament probe so it is as close as possible to the diamond membrane, which is > 300 μm from the diamond membrane due to the thickness of the silicon frame the diamond is mounted on. However, we do not want the filament probe to touch the Si. We will then pump down both sides of the diamond membrane and cool it down. For this test the electron gun will be operated in a pulsed mode, so as to not unnecessarily stress the diamond membrane. The filament probe is wired to

a coaxial cable in vacuum, and this coaxial cable will connect the probe to a pico-ammeter, from which we can positively bias the filament probe so that the electrons are attracted to the filament, collecting any electrons that scatter off of the diamond membrane. From the pico-ammeter we will also get an oscilloscope reading of the voltage in through the filament probe. We can subtract out the DC offset that positive biasing gives us and resolve the current through the wire, knowing the resistance in the system.

With this pico-ammeter, we will resolve out the loss in the system. We expect between 15-30% transmission, as the SiN membrane in the Mühlberger groups excimer lamp [15, 16] transmitted 30% of the electrons, but our diamond membrane is 500 nm thick compared to the 300 nm thick Mühlberger group's SiN membrane. By subtracting the current seen by the pico-ammeter from the Emission Current readout on the electron gun power supply system, after subtracting out the positive bias and accounting for the resistance in the wires, we will be able to characterize the electron transmission characterization.

3.3 Electron Mean Free Path Characterization

To characterize the mean free path of the electrons in Ar and compare the scattering cross section to previous experimental measurements following our determination of the electron transmission, we will pump .5 atm of Ar into the excimer decay chamber with the filament probe attached, positively biased, and still as close to the diamond membrane as possible without touching the Si ($\sim$300 μm). From here we will use a pulsed electron beam with a low current at electron energies starting at 1 KeV and iterate through the highest attainable electron energy with our system (which is as of yet indeterminate due to the use of the VSW HV power supply). The total cross section of electron atom collisions maxed out at electron energies of $\sim$15 eV, then decreases as electron energy decreased [18]. However, only electron energies up to 1 KeV were measured.

The mean free path is defined as the length at which only $\frac{1}{e}$ of the initial intensity remains.

Explicitly, transmitted intensity A_t goes as:

$$A_t = \frac{A(x)}{A_0} = e^{\frac{-x}{\ell}} \tag{3.1}$$

where A is the intensity, x is the depth into the gas, and ℓ is the mean free path, also defined as

$$\ell = (n\sigma)^{-1} \tag{3.2}$$

where n is the number of target molecules per unit volume or number density, and σ is the scattering cross section. Solving for number density is simply a rearrangement of the Ideal Gas Equation:

$$n = \frac{N}{V} = \frac{P}{k_B T} \tag{3.3}$$

where N is the number of particles, V is the volume, P is the pressure, k_B is Boltzmann's constant and T is temperature. Intensity A is related to current I through power in that

$$\text{Power} = I(x)^2 R = \int A \cdot \, d^2 r = A(\pi r_a^2) \tag{3.4}$$

where R is the resistance in the system, $I(x)$ is the distance dependent current resolved from the pico-ammeter, and r_a is the spot size of the electron beam, which we will tune to the radius of the aperture drilled into the copper window frame (.0118" or .300 mm). We are approximating a uniform beam as opposed to a gaussian beam, but this should not matter as the filament is positively biased, making any electrons in the area attracted to it. The positive bias also serves to repel any ionized Ar molecules that are formed during the excimer decay process, of which there are many [12]. Rearranging, we can solve for the scattering cross section as:

$$\sigma = \frac{-k_B T x}{P \ln(\frac{I(x)^2 R}{\pi r_a^2})} \tag{3.5}$$

Equation 3.5 may seem like σ has an odd x dependence, but because current decays exponentially as a function of x as well, those distance dependences cancel out and we get a constant value. This constant value will not be valid for high electron energies when excimer light is generated, as excimer light is high enough energy such that the filament might photoemit, causing the filament to lose electrons to the surrounding gas, skewing our data. Therefore, the values for the scattering

cross section will only be valid below the threshold of photoemission. However, characterizing the mean free path of electrons in Ar while excimer decay is occurring is pivotal for effectively implementing optics that capture the most of the solid angle, and as such, once we verify our 1 KeV results with the data provided in [18], we will be able to make a trendline of σ vs electron energy with a large dataset. We can also resolve the photoelectric effect out of our signal after determining the work-function of our filament probe and cross reference the trend line with the photoelectric effect resolved values.

Chapter 4

Conclusions and Outlook

4.1 Diamond Membrane Viability for Use in Excimer Technology

This research project is ongoing, and as such, we have yet to determine whether this Novel High-Brightness EUV/VUV Excimer Light Source is viable or not. This chapter will describe the future work of developing a permanent system following the proof of concept and preliminary tests outlined in Chapter 3, as well as provide a broader scope for this project in terms of excimer technology as a whole.

4.2 Future Work

Future work in this project will be designing a system that can fire VUV directly into our ARPES system and focus to a point on an ARPES sample. The system design will be exactly the same as described in this thesis for everything on the vacuum side of the diamond membrane, but the excimer side will need to feature a LiF (see Section 2.7.3) barrier that can hold vacuum such that EUV/VUV can be fired into the requisite vacuum for ARPES.

This LiF barrier can be either a lens or a window, and each would optimize different facets and depends upon the results of Section 3.3. Regardless of whether or not a window or lens is used, another lens would need to be purchased so as to focus the light to a point on the ARPES sample. In this sense, using a LiF window as the barrier that holds back the ARPES vacuum is cost effective (LiF windows are significantly cheaper than LiF lenses), and because LiF is prone to developing optical defects, only needing to replace a window and a lens as opposed to two lenses

is cheaper. However, while the lens-window combination is cost effective, VUV intensity is lost as compared to the two lens method because a LiF window will not focus the VUV and more of the 4π steradians of light will be lost.

Two lenses would entail fixing an LiF lens that holds vacuum into place with a focal length such that it gathers the largest amount of solid angle possible while also having a broad enough depth of focus to accurately collimate light such that it can be focused down by the second lens to a tight point on the ARPES sample. Thus, using a lens provides its own set of problems. The first of these problems is misalignment. If the lens is extremely close to the point light source, the depth of focus will be very small and prone to misalignment. When tightening conflats with copper gaskets, the size of a chamber may increase with the thickness of the copper gasket and the tightness of the bolts. Therefore, if we use two LiF lens we would need to optimize the distance from the source of light to the LiF lens in terms of depth of focus and solid angle so that the system is not prone to misalignment while also collimating as much of the solid angle as possible. Using a lens requires a very accurate reading of the electron mean free path in Ar, one that tells us precisely where the excimer light originates, and if a good reading cannot be obtained as described in Section 3.3, using a LiF lens as the optical element that holds vacuum is a futile pursuit. We might also consider using the window-lens design with a parabolic mirror as used by the Muhlberger group [16].

In order to fasten a LiF optical element—be it a window or a lens—such that it holds vacuum, we will design and order a specialized stainless steel conflat that is capable of making a seal against the optical element with a gasket. This will allow the optical element to hold vacuum.

4.3 Project Scope Beyond ARPES

This project has a much larger scope beyond the niche application we will use it for in ARPES. In the last 20 years, excimer technology usage has grown exponentially, finding both industrial and RD applications in a wide range of fields, particularly in Micro-electro-mechanical systems and lithographic processes. Excimer technology is advantageous for many of these processes owing to the precision gained from its short wavelength [5]. In the examination of ncD membranes as viable

for use in excimer technologies, we stand to provide a more durable, more CW-operable alternative to silicon nitride membranes in similar systems, as well as show that CVD Diamond is a viable material for use in excimer technology as a whole.

4.3.1 A Biophysical Application

Recently, the field of oncology has begun developing uses for excimer technology, and while the medical applications of excimer technology are growing slower than industrial fields [5], the prospects look good. UV light generates biological changes in living organisms, and germicidal UV (254 nm) generated by a low-pressure mercury lamp has a wide range of applications today. This type of light falls within the range of UV-C light (100-280 nm), and this germicidal function is achieved by causing dimers to form in the bacterial DNA. Thymine dimers occur when neighboring thymine molecules in DNA covalently bond, causing a kink in the double helix structure; this process can also occur between a thymine and a cytosine (pyramiding dimers). While reading this DNA, the cell will notice these dimers and attempt to repair them with excision repair or photoreactivation (a process which requires the protein Photolyase, which animals generally lack) [20].

If the cell is unable to repair its DNA, cell death is triggered. There are two types of cell death: necrosis and apoptosis. Necrosis and apoptosis differ in control; necrosis is considered uncontrolled cell death, where a cell simply explodes, potentially harming neighboring cells, whereas apoptosis is controlled cell death in which a cell essentially implodes, leaving neighboring cells unharmed [22].

When a cell is damaged such that it cannot undergo apoptosis, it becomes tumorous and potentially cancerous. A major focus in oncology research is the ability to trigger apoptosis by some biological pathway. The dynamics of this process are not understood completely, but studies have shown that the tumor suppressing protein p53 plays an extremely important role in triggering apoptosis [23] as well as DNA excision repair [22]. As such, many oncology research avenues look for ways to actively manipulate this protein.

Conventional radiation therapies use x-ray radiation to non-invasively target cancer and cause double stranded breaks in the DNA—where the bond connecting two complementary nucleotides

is broken, which usually causes the DNA to undergo apoptosis.

Many studies have shown that UV-C is capable of activating p53 to trigger apoptosis [2, 9, 22], and that UV-C is even capable of triggering apoptosis in p53-deficient cells [22]. In fact, the University of Tokai recently demonstrated that a wide-band UV-C (230-280 nm) Pulse Flash Ray (UVCPFR) irradiation technique not only triggers apoptosis in tumorous cells, but it selectively triggers apoptosis in tumorous cells, leaving healthy cells roughly unharmed (see Figure 3.1) [9, 17] This technique utilizes a Xenon excimer lamp to generate this broad band signal, and they are currently developing an apparatus to exploit this selectivity [9].

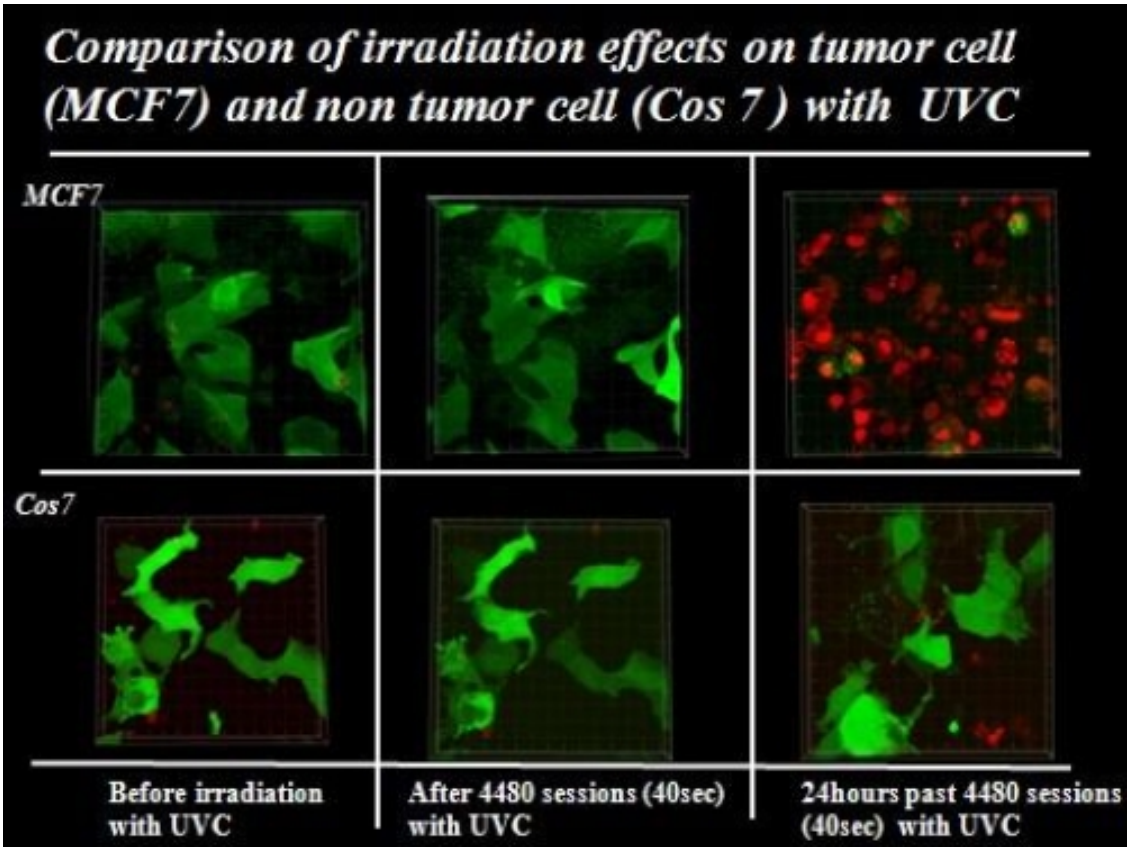

Figure 4.1: A graphic illustrating the selectivity of UVCPFR; UV-C only damages tumorous cells and barely harms healthy cells [17]

While the development of a high-brightness light source described by this thesis may not have a readily apparent 1-1 correlation with this biophysical application, it may very well aid future development of medical apparatuses. The use of CVD diamond in excimer technology might

increase the lifetime of these technologies, and a future application such as this might exploit CVD diamond to increase the lifetime of an apparatus, which is particularly valuable in a medically disadvantaged setting such as a 3rd world or developing country. As such, the wide field of excimer technology stands to benefit from this exploration of CVD Diamond.

Bibliography

[1] A. A. Abrikosov. Type ii superconductors and the vortex lattice. Nobel Lecture, December 2003.

[2] M. L. Agarwal*. Photodynamic therapy induces rapid cell death by apoptosis in l5178y mouse lymphoma cells. Cancer Research, 51:5993–5996, November 1991.

[3] R. S. Balmer*. Chemical vapour deposition synthetic diamond: materials, technology and applications.

[4] J. Bardeen*. Theory of superconductivity. Physical Review, 108(5):1175–1204, December 1957.

[5] D. Basting*. History and future prospects of excimer laser technology. RIKEN Review, (43):14–22, January 2002.

[6] L. N. Cooper. Bound electron pairs in a degenerate fermi gas. Physical Review, 104(4):1189–1190, November 1956.

[7] A. Damascelli. Probing the electronic structure of complex systems by arpes. Physica Scripta., T109:61–74, 2004.

[8] T. Hanaguri*. Coherence factors in a high-tc cuprates probed by quasi-particle scattering off vortices. Science, 323:923–926, February 2009.

[9] J. Itoh. Method for killing tumor cells selectively and apparatus for the method. European Patent Office, September 2012.

[10] Kimball Physics, 311 Kimball Hill Road, Wilton, NH 03086, USA. EMG-4210/EGPS-4210 Electron Gun and Power Supply System, April 2013.

[11] J. D. Koralek*. Experimental setup for low-energy laser-based angle resolved photoemission spectroscopy. Review of Scientific Instruments, 78(053905), May 2007.

[12] D. C. Lorentz. Excimer formation and decay processes in rare gases. Prepared for: Office of Naval Research, September 1973.

[13] Crystran Ltd. Lithium flouride data sheet. Elecronic.

[14] Diamond Materials. The cvd diamond booklet. Electronic, 2008.

[15] F. Muhlberger*. Single photon ionization (spi) via incoherent vuv-excimer light: Robust and compact time-of-flight mass spectrometer for on-line, real-time process gas analysis. Anal. Chem., 74:3790–3801, 2002.

[16] F. Muhlberger*. Single-photon ionization quadrupole mass spectrometry with an electron beam pumped excimer light source. Anal. Chem., 77:2218–2226, 2005.

[17] Tokai University School of Medicine. New cancer therapy using ultra-violet c (uvc) pulse flash irradiation. ScienceDaily, August 2012.

[18] G. G. Raju. Electron-atom collision cross sections in argon: An analysis and comments. IEEE Transations ond Dielectrics and Electrical Insulation, 11(4):649–673, August 2004.

[19] D. K. Reinhard*. Fabrication and properties of ultranano, nano, and microcrystalline diamond membranes and sheets. J. Vac. Sci. Technol. B, 22(6):2811–2817, Nov/Dec 2004.

[20] R. P. Sinha*. Uv-induced dna damage and repair: a review. Photochem. Photobil. Sci., 1:225–236, March 2002.

[21] Space Environment Technologies. Iso 21348 definitions of solar irradiance spectral categories.

[22] M. T. Tomicic*. Apoptosis in uv-c light irradiated p53 wild-type, apaf-1 and p53 knockout mouse embryonic fibroblasts: Interplay of receptor and mitochondrial pathway. Apoptosis, 10(6):1295–1304, 2005.

[23] JYJ Wang. Dna damage and apoptosis. Cell Death and Differentiation, 8(11):1047–1048, November 2001.

NOTE: * indicates et. al.